Synthesis and analysis of poly(*t*-butyl methacrylate)-*b*-poly(vinylidenefluoride-*r*-trifluoroethylene)-*b*-poly(*t*-butyl methacrylate) block copolymers

Mellema, H.H.; Meereboer, N.L.; Loos, K.; ten Brinke, G.;
Department of Polymer Chemistry, Zernike Institute of Advanced Materials, University of Groningen, 2015

university of groningen

BSC Thesis 2015

Synthesis and analysis of poly(*t*-butyl methacrylate)-*b*-poly(vinylidenefluoride-*r*-trifluoroethylene)-*b*-poly(*t*-butyl methacrylate) block copolymers

Mellema, H.H.; Meereboer, N.L.; Loos, K.; ten Brinke, G.;
Department of Polymer Chemistry, Zernike Institute of Advanced Materials, University of Groningen, 2015

Abstract: *The ferroelectric P(VDF-TrFE) polymer is of great interest for multiple applications including memory devices. However the effect of nanoconfinement on the curie transition is still being investigated. In this report we synthesized PtBMA-b-P(VDF-r-TrFE)-b-PtBMA block copolymers by first synthesizing a P(VDF-TrFE) macroinitiator using radical polymerization, and subsequently synthesizing the block copolymers using atom transfer radical polymerization (ATRP). The resulting block copolymers were studied using 1H-NMR, differential scanning calorimetry and polarized optical microscopy in order to study the effect of block copolymer confinement on the curie transition. A kinetics study was done to investigate the effectiveness of ATRP for creating these block copolymers.*

Contents

Introduction

Ferroelectricity

When some materials are put under an electric field, they experience a linear polarization that is proportional to the electric field, an effect that is called dielectric polarization[1]. Some materials react more strongly to the electric field, producing a non-linear polarization called paraelectricity[1]. Ferroelectricity is different from these two phenomena in that a ferroelectric material can retain some of its polarization even after the electric field is removed, and that the polarization can be switched by reversing the electric field which results in a so called hysteresis loop (Figure 1)[2].

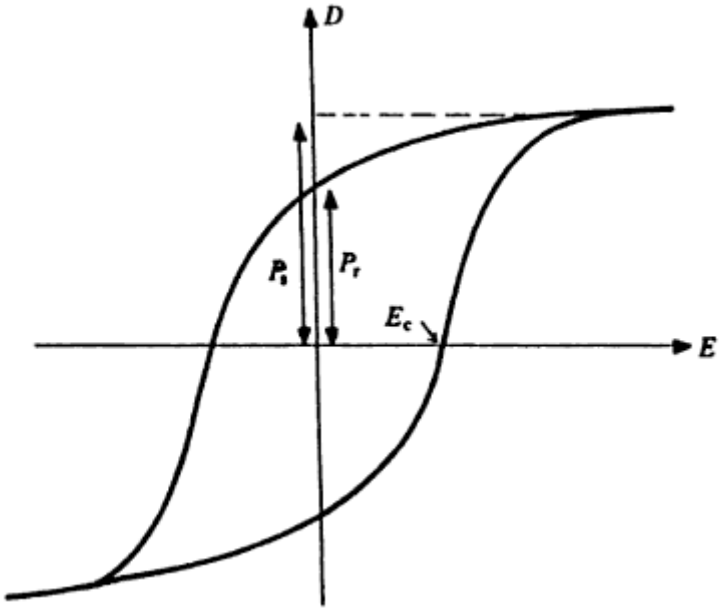

Figure 1: Ferroelectricity

Ferroelectric behavior is temperature dependent, once the material reaches a certain temperature the material loses its ability to retain polarization and it will instead demonstrate paraelectric behavior. The temperature at which this happens is dependent on the material and is called the Curie temperature (T_c)[2].

Due to the nature of ferroelectricity, ferroelectric materials also exhibit piezoelectric (ability to generate voltage under mechanical stress)[1] and pyroelectric (ability to generate voltage under temperature changes)[1] behavior. Ferroelectric materials are already used as actuators, transducers[3] and sensors[4] while ferroelectric memory[5] and multiferroics[6] are current fields of research.

PVDF and its ferroelectric properties

Polyvinylidene fluoride (PVDF, $-(C_2H_2F_2)_n-$) was discovered to have piezo electric properties in 1969, and two years later it was also found to have ferroelectric properties. A number of other ferroelectric polymers have been found (odd-nylons[7], cyanopolymers[8]), however PVDF excels due to its stability, high compact structure and its large dipole moment[9].

The origin of PVDF's ferroelectricity lies in its chain conformations. PVDF can crystallize in numerous phases with each having a different conformation depending on the amount and order of trans and gauche bonds. The two most common conformations are the alpha (α) phase (with conformation *tg^+tg)* and the beta (β) phase (all-trans, *tttt*) (Figure 2)[10].

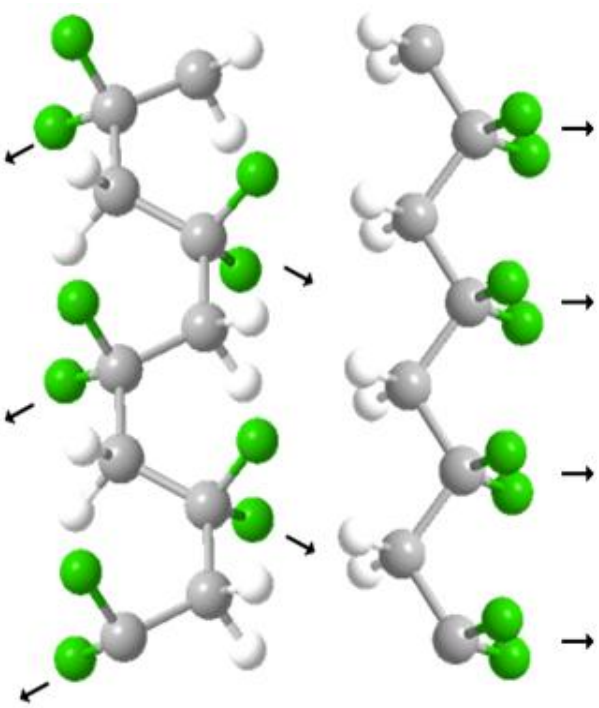

Figure 2: α-phase (left) and β-phase (right) of PVDF

PVDF, regardless of its conformation, contains dipole moments due to the C-F bonds in the material. In the α-phase, these dipoles alternate in direction which result in the net dipole of the whole chain is cancelled out. However, these polymer chains tend to pack together in such a way that the dipoles of the chains cancel each other out[10]. In the β-phase the dipole moment of each monomer unit points in the same direction, which results in the whole chain having a large dipole perpendicular to the polymer chain. Therefore, the crystalline β-phase allows PVDF to be ferroelectric[10]. However PVDF tends to crystallize in the α-phase, so further processing (straining, stretching, or quenching) is required to increase the amount of the β-phase and improve the ferroelectric properties of the material[11, 12].

These different conformations can also be used to explain the Curie temperature. When heated above this temperature the bonds of the β-phase change conformation from *tg^+tg* into the all-trans conformations of the α-phase, causing the dipole moments to alternate and cancel out, thus changing the properties of the material from ferroelectric to paraelectric[10]. However, despite PVDF being a ferroelectric material, it does not have an observable Curie temperature. PVDFs Curie temperature was calculated to be 205°C, about 20°C above its melting temperature[9, 10].

P(VDF-T*r*FE) copolymer

Poly(vinylidene fluoride-*co*-trifluoroethylene) is a random copolymer similar to PVDF except using two monomers instead of one (Figure 3)[13]. The extra fluorine atom of the second monomer adds extra steric hindrance to the chain of P(VDF- T*r*FE). If the amount of T*r*FE is high enough, the steric hindrance will force the copolymer to crystallize almost completely in the ferroelectric β-phase instead of the α-phase[10].

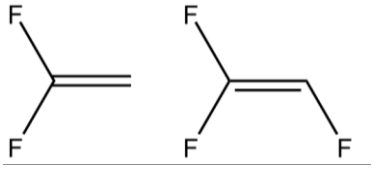

Figure 3: vinylidene fluoride and trifluoroethylene

While P(VDF-tRFE) is readily ferroelectric and does not require additional processing, it also differs from PVDF in a number of ways. First, the extra fluorine replaces a hydrogen and so slightly reduces the overall dipole moment[9]. T*r*FE is also a more hazardous and expensive monomer compared to VDF[13]. The biggest difference is that P(VDF-T*r*FE) has an observable curie transition. While the melting temperature of P(VDF-T*r*FE) is the lowest at 80% VDF content, the curie temperature drops proportional to the amount of T*r*FE, which causes the curie temperature to appear at about 85% VDF content[14]. This proportional relationship was used to extrapolate the curie temperature of PVDF[15].

P(VDF-T*r*FE) has been shown to have a double Curie transition[16]. This can be explained by temperature dependence of the crystallization rate of the alpha and beta phases (Figure 4). When P(VDF-T*r*FE) is heated above its melting temperature and is cooled down, it will crystallize into alpha phase first. Cooling down further, the crystallization will produce less alpha phase and more beta phase until only beta phase is produced and the crystallization finishes. Because the steric hindrance of the added T*r*FE aids the formation of beta phase, when the temperature of the material is below the Curie temperature any alpha phase will transform into beta phase. However these chains will not transform completely, causing the resulting beta phase to have many trans-gauche defects. The resulting material will have two distinct beta phases, β_1-phase which is produced by crystallization and β_2-phase which was originally α-phase, each with their own distinct Curie transition[16].

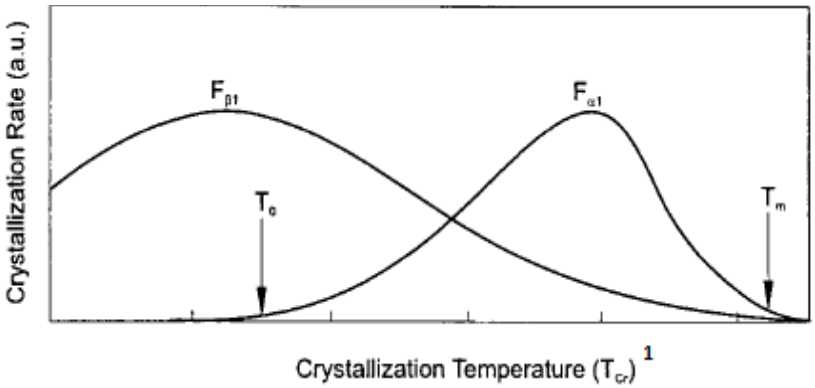

Figure 4: Crystallization rate of P(VDF-T*r*FE)

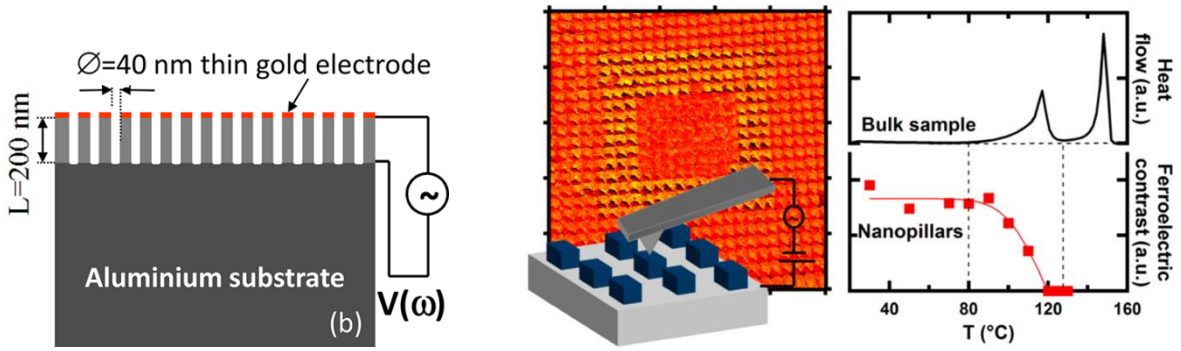

Figure 5: Serghei et al. (left)and Kassa et al. (right)

While the curie temperature of bulk P(VDF-T*r*FE) is well understood, the effect of scaling down the amount of material on the Curie transition is still investigated[17, 18]. Serghei et al.[19] reported that attograms of P(VDF-T*r*FE) in nanocontainers showed a reduction in curie temperature compared to bulk while Kassa et al.[20] reported that freestanding nanopillars of P(VDF-T*r*FE) showed almost no reduction (<10°C). A low curie temperature is useful for certain applications like actuators; however for applications that rely solely on the ferroelectric behavior (e.g. memory) it is a problem, since a device that relies on such a material will fail if it loses it ferroelectric properties. If the curie temperature drops significantly when the amount of P(VDF-T*r*FE) is reduced it would put a limit on the usefulness of the material. Besides the previously mentioned ways to create nanoconfined P(VDF-T*r*FE), it is also possible to utilize block copolymer self-assembly.

Block Copolymers

Block copolymers consist of multiple homopolymers that are connected to each other with covalent bonds[21]. One interesting property of block copolymers is that they can undergo 'microphase separation', in which the different blocks separate into different phases (like water and oil). However due to the blocks of the copolymer chain being connected to each other they cannot macrophase seperate, instead they form complex phases on a molecular scale (5-100 nm). This process is also known as block copolymer self-assembly[22].

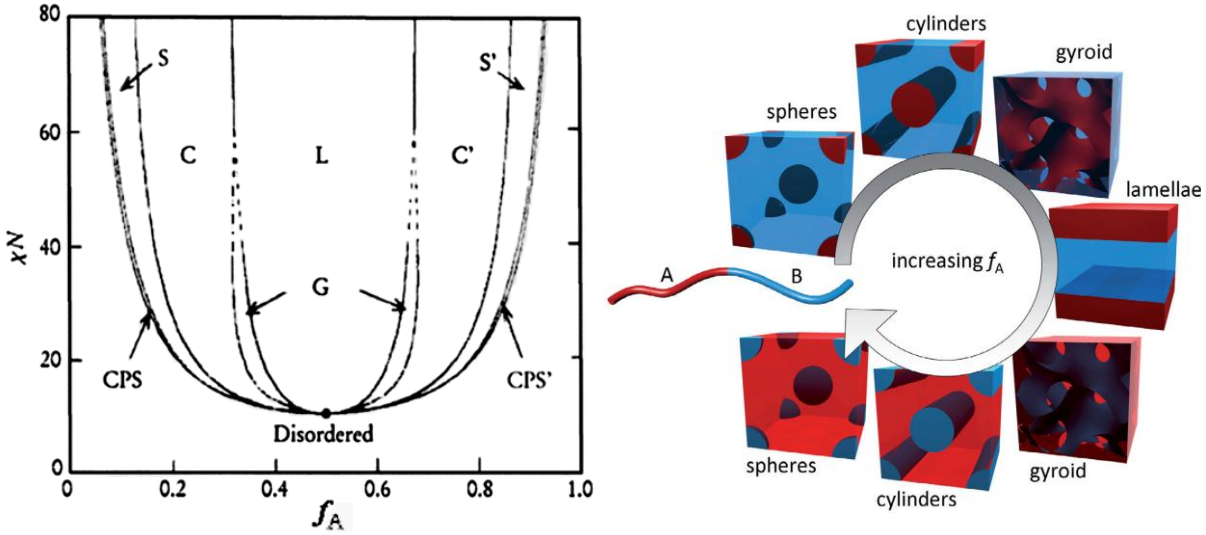

Figure 6: Theoretical phase diagram for linear AB diblocks and the different possible morphologies

Microphase separation is controlled by three factors: *N* is the average segment lenght of the block copolymer, the fraction of block *A* per chain (f_A), and the Flory-Huggins interaction parameter χ_{AB} which describes the interaction between monomers. Positive χ_{AB} indicates net repulsion between monomers A and B while a negative value indicates a tendency to mix. χ_{AB} is also inversely proportional to the temperature, meaning a higher temperature will promote mixing. The theoretical diagram of the possible phases for AB block copolymers is shown in Figure 6. When the value of χN is lower that 10,5 (due to either small polymer chains or weak interaction) or when the fraction of one of the blocks is very small there is no micro phase separation (the disordered state). When χN is large enough and f_A is around 0,5 the polymer separates into a lamellar structure. Increasing the fraction of one of the blocks will change the morphology to gyroids, cylinders and then spheres before becoming disordered. Higher values for χN causes the confinement to become stronger as well as the disappearance of the gyroid morphology[21].

It is important to note these morphologies can only be achieved under certain conditions. If the glass transition temperature of block A is be higher than the crystallization temperature of block B, the crystallizing block B will be confined within the glassy domains of Block A. If the crystallization temperature is higher these microphases are only possible if there is strong segregation as well as an excess of the glassy block A compared to the crystalline block B. Otherwise the crystallization dominates and the only phase that forms is a lamellar microphase within larger spherulites structures.[23]

While diblock copolymers have only a few morphologies, many more can be found by increasing the amount of blocks and by changing the way blocks are connected (linear, branched, star)[24]. This complicates the phase diagram significantly due to three interaction parameters ($\chi_{AB}, \chi_{AC}, \chi_{BC}$), two fraction parameters (f_A, f_b) and even architectural parameters for different block sequences and chain architecture[25].

Flory-Huggins theory uses lattice theory and assumes that both blocks are perfect coils. Polymers that are more rod like[26] as well as crystalline polymers[27] significantly alter this behavior compared to theoretical diblock polymers, but still allow morphologies.

There are a multitude of ways to fabricate block copolymers containing P(VDF-T*r*FE) segments. Among these are conventional radical polymerization, azide alkyne click chemistry and controlled radical polymerizations like atom transfer radical polymerization (ATRP), reversible addition–fragmentation chain transfer (RAFT)[28] and macromolecular design via the interchange of xanthates (MADIX) polymerizations and Iodine transfer polymerization (ITP)[13, 29, 30]. This report will focus on ATRP.

Atom transfer radical polymerization

Radical polymerizations are useful reactions due to their tolerance to functional groups as well as impurities, and it has been the leading industrial method to produce polymers. It is however an uncontrolled reaction and termination occurs randomly leading to high polydispersity[31]. Unlike conventional radical polymerizations, Atom transfer radical polymerization (ATRP) is a form of controlled radical polymerization (CRP)[30]. The basis of all CRP methods is the same; by establishing an equilibrium between a small amount of active growing radical chains and a large amount of dormant species.

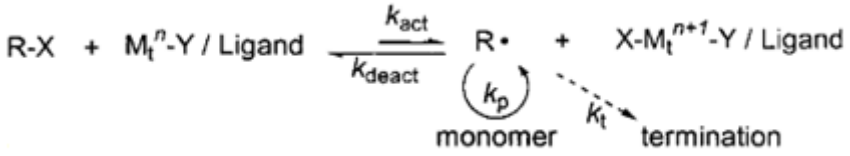

Scheme 1: Transition metal-catalyzed ATRP

The first thing required for a successful ATRP reaction is a halogen terminated initiator. A reversible redox process is used to establish an equilibrium between the halogenated initiator and a radical species. A metal complex is used to catalyze this redox process. Ligands are required in order to make the metal species soluble. The generated radical species can react in a number of ways. It can react back to a halogenated species, react with a monomer molecule (creating a new radical) or it can terminate. However due to the established equilibrium the amount of radical species and thus the amount of termination will be very low (a few percent), meaning ATRP behaves as a pseudo-controlled reaction. The termination at the beginning of the reaction usually does not exceed 5% of the total amount of growing chains. This early termination generates the oxidized metal complex in order to reduce the concentration of growing chains and so reduce the amount of termination. A successful ATRP reaction requires fast initiation as well as a fast equilibrium and will have a small contribution of terminated chains as well as uniform chain growth.[30]

Aim of the research

The goal of this project is synthesize nanoconfined P(VDF-T*r*FE) in a P*t*BMA matrix. P*t*BMA was chosen due to its high glass transition temperature compared to the crystallization temperature of P(VDF-T*r*FE), as well as its use as a monomer for subsequent ATRP. A P(VDF-T*r*FE) macro initiator will be synthesized (Scheme 1)[32] where we will aim for a VDF/T*r*FE ratio that causes the overall crystallization temperature to drop below the T_g of P*t*BMA as well as to show clear Curie transitions. The following ATRP reaction will utilize a CuCL/PMDETA complex in order to synthesize the P*t*BMA-*b*-P(VDF-*r*-T*r*FE)-*b*-P*t*BMA block copolymers (Figure 7)[32]. These will be studied using ^{1}H-NMR spectroscopy, differential scanning calorimetry (DSC), polarized optical microscopy (POM), Fourier transform infrared spectroscopy (FTIR) and gel permeation chromatography (GPC).

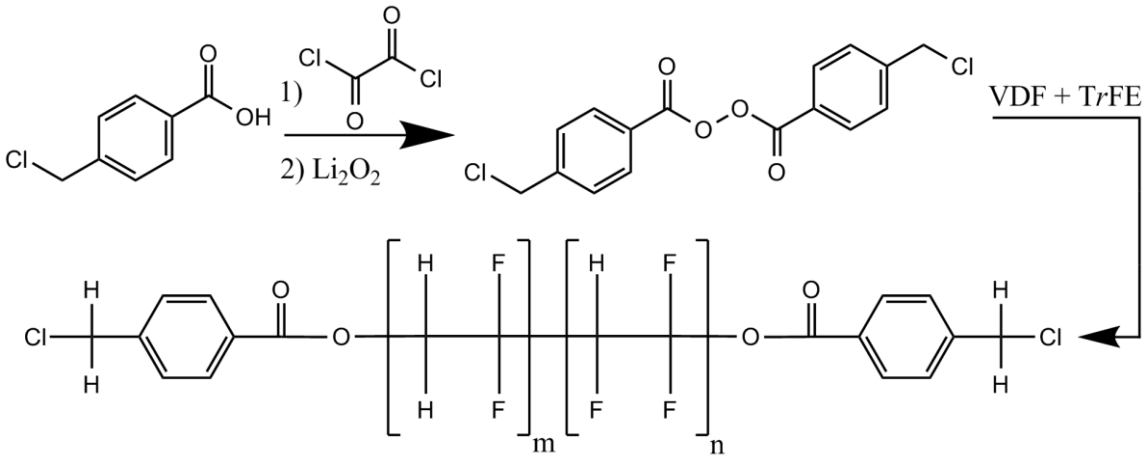

Scheme 2: P(VDF-r-TrFE) synthesis

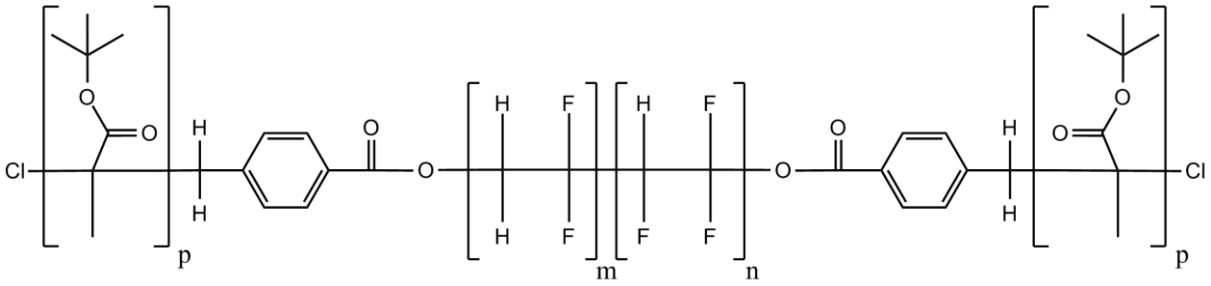

Figure 7: PtBMA-b-P(VDF-r-TrFE)-b-PtBMA block copolymer

Experimental

tert-Butyl methacrylate (*t*BMA,Aldrich,98%) was dried overnight under N_2 atmosphere over CaH_2 and condensed with liquid nitrogen (10^{-2} mbar), Oxalyl chloride (Acros, 98%), 4-(chloromethyl)benzoic acid (Acros, 98%), lithium peroxide (Li_2O_2, Acros, 95%), vinylidene fluoride (VDF, Synquest Labs, 98%), trifluoroethylene (T*r*FE, Synquest labs, 98%), copper(I)chloride (CuCL, Acros, 99,99%), 1,1,4,7,7-pentamethyldiethylenetriamine (PMDETA, Acros, 99+%), p-Toluenesulfonyl chloride (p-TSCl, Sigma-Aldrich, >99%), anhydrous dimethylformamide (DMF, Across, 99%), anhydrous acetonitrile (Across, 99%), anhydrous toluene (Across, 99%) and anhydrous dichloromethane (DCM, Across, 99%) were used as received. All solvents used were of HPLC grade.

Synthesis of 4-(chloromethyl)benzoyl peroxide

4-(chloromethyl)benzoic acid (10 g, 59 mmol) was dissolved in 50 ml of anhydrous DCM and stirred at 0°C under N_2 atmosphere. Oxalyl chloride (5.4ml, 63 mmol) and six drops of anhydrous DMF were added to the stirred solution. After reacting for 2 h at room temperature, the solvent was removed by rotary evaporation and the remaining yellow residue was immediately dissolved in 100 ml n-hexane/Et_2O (1:1). The resulting solution was slowly added via a droplet funnel to a rapidly stirred 50 ml aqueous solution of Li_2O_2 (3.5 g, 75 mmol) at 0°C. After reacting for 2 h at room temperature, the reaction mixture was diluted with 500 ml chloroform and washed twice with H_2O. The organic phase was filtered and removed by rotary evaporation. The remaining white solid was dissolved in chloroform and dried on $MgSO_4$, after which the solvent was removed by rotary evaporation at 40°C until crystallization started. The mixture was stored overnight at 6°C and then filtered over a glass filter yielding 2.22 g (6.546 mmol, 22.2%) white needle-shaped crystals. ^{1}H-NMR (400 MHz, $CDCL_3$, δ): 8.08 (d, 4H, -Ar<u>H</u>), 7.55 (d, 4H, -Ar<u>H</u>), 4.64 (s, 4H, -PhC<u>H_2</u>Cl).

Synthesis of chlorine-terminated P(VDF- T*r*FE)

A solution of 4-(chloromethyl)benzoyl peroxide (0.5 g, 1.5 mmol) in 300 ml anhydrous acetonitrile was added to a pressure reactor (Parr Instruments, model 4568). The vessel was closed and purged with nitrogen for 30 min to degas the mixture. Subsequently, the reactor was charged with 2.81 bar of T*r*FE and afterwards 15 bar of VDF, heated to 90°C and stirred at 500 rpm. After reacting for 30 min, the vessel was cooled down to room temperature and depressurized. The solvent was removed by rotary evaporation and the remaining solid was dissolved in 20 ml DMF and precipitated in 400 ml MeOH/H_2O (1:1). The remaining solid was washed thoroughly with chloroform and dried in vacuo in an oven, yielding an off-white solid. This solid was then precipitated again from 20 ml DMF added in 400 ml MeOH/H_2O (1:3) and then washed thoroughly with chloroform yielding an off-white solid. A Soxhlet extraction was performed to remove final traces of initiator, yielding 4.03 g white solid. ^{1}H-NMR (400 MHz, DMSO, δ): 8.01 (d, -Ar<u>H</u>), 7.66 (d, -Ar<u>H</u>), 7.61 (d, -Ar<u>H</u>), 5.43, (m, -CF_2-C<u>H</u>F-CF_2-, T*r*FE), 4.84 (s, 4H, -PhC<u>H_2</u>Cl), 2.91, (m, -CF_2-C<u>H_2</u>-CF_2-, VDF head-to-tail), 2.68, (m, -CF_2-C<u>H</u>F-CH_2-, VDF), 2.27 (m, -CF_2-C<u>H_2</u>-CH_2, VDF)

Synthesis of P*t*BMA-*b*-P(VDF-*r*-TrFE)-*b*-P*t*BMA

A dried Schlenk tube sealed with rubber septum was put under nitrogen atmosphere after which chlorine-terminated PVDF (0.39 g, 0.03 mmol) and CuCl (50 mg, 0.50 mmol) were added, followed by evacuating and backfilling three times with nitrogen. A degassed syringe was used to add anhydrous DMF (5.0 ml), PMDETA (0.31 mL, 1.5 mmol) and lastly *t*BMA (2.84 mL, 17.5 mmol). The reaction mixture was immediately subjected to four freeze-pump-thaw cycles to degas after which the Schlenk tube was put in an oil bath at 75°C. The mixture reacted for a desired amount of time, after which the mixture was cooled down in a water bath. The dark-brown mixture was precipitated in MeOH/H_2O (100 mL, 1 : 1) and the greenish solid was collected by filtration and dissolved in acetone, after which the solvent was rotary evaporated. Reprecipitation was carried out twice from 4ml DMF in MeOH/H_2O (40 : 60), and the collected off-white solid was dried in a vacuum oven overnight. ^{1}H-NMR (400 MHz, Acetone-d_6, δ): 5.45 (m, -CF_2-C<u>H</u>F-CF_2-, TrFE), 3.05 (m, -CF_2-C<u>H_2</u>-CF_2-, VDF head-to-tail), 2.40 (m, -CF_2-C<u>H_2</u>-CH_2, VDF), 1.92 (m, -C<u>H_2</u>C(CH_3)(COOtBu)-), 1.53 (m, CH_2C(CH_3)(COO<u>tBu</u>)-), 1.13 (m, CH_2C(<u>CH_3</u>)(COOtBu)-).

Synthesis of P*t*BMA

A dried 100 mL three-necked flask was degassed (i.e. by evacuating and backfilling with nitrogen three times). To this flask CuCl (0.091 g, 0.92 mmol) was added and it was evacuated and backfilled another three times. *t*BMA (4.5 mL, 0.28 mmol), toluene (4 ml), and PMDETA (0.194 mL, 0,926 mmol) were added using degassed syringes and the mixture was stirred. The Schleck tube was put into a thermostated oil bath at 90 °C. At the same time pTsCl (0.881 g, 4.62 mmol) was added to a dried and degassed 50 mL three-necked flask and was degassed again, after which toluene (10 ml) was added via a degassed syringe. 2 ml of this initiator solution was added to the Schleck flask, and the polymerization was carried out for 5 h. Next, the mixture was dissolved in THF and passed through a basic alumina column to remove copper species. The solvents were evaporated, and the polymer was precipitated in a 10-fold excess of cold hexane (-60 to -50 °C). The polymer was collected by filtration. Finally, the polymer was dried in a vacuum oven overnight.

Characterization

^{1}H nuclear magnetic resonance (^{1}H-NMR) spectra were recorded on a 400 MHz Varian VXR at room temperature. Differential Scanning calorimetry (DSC) was done using a TA instruments Q1000 in N_2 atmosphere with a range of -40°C to 200°C and a heating/cooling rate of 10°C. Polarized optical microscopy (POM) was done on a Zeiss Axiophot and the samples were placed between crossed polarizers. Fourier transform infrared (FTIR) spectroscopy measurements were taken using a Bruker IFS88 spectrometer equipped with MCT-A detector at a resolution of 4 cm^{-1}. Gel permeation chromatography (GPC) was performed in DMF (1 ml/min) with 0.01 M LiBr on a Viscotek GPCMAX. Molecular weights were calculated via universal calibration using narrow disperse polystyrene standards (Polymer Laboratories).

POM Samples

Polarized optical microscopy samples were prepared by dissolving 10 mg of material in a few drops of DMF, after which a drop of this concentrated solution was placed on a glass plate that was heated to 80°C. The resulting plates were put under the microscope in a heating device and the samples where heated to 200°C before being cooled down back to room temperature.

Blends

The blends where prepared by mixing homopolymer P*t*BMA with the P(VDF-T*r*FE) macroinitiator to a total weight of 40 mg, which was then dissolved in DMF for both POM samples as well as DC samples. The prepared P*t*BMA/P(VDF-T*r*FE) blends did have the following weight ratios: 50/50, 60/40, 70/30 and 80/20.

Results and Discussion

Synthesis of P(VDF-T*r*FE) macroinitiator

A radical initiator was required to synthesize the P(VDF-T*r*FE) macroinitiator. 4-(chloromethyl)benzoyl peroxide was synthesized using the procedure described previously. The low yield is due to loss of product that was still dissolved. The filtered solution was rotary evaporated and stored in a freezer in case more is required.

For the synthesis of P(VDF-T*r*FE), in order to reach a ratio of VDF-T*r*FE with a clear Curie transition, pressures of 2,81 bar and 15 bar were used. Unfortunately after washing the product it was still impure so it was reprecipitated and washed again, but with no effect. Finally a Soxhlet extraction was done overnight, whereafter ^{1}H-NMR spectroscopy confirmed the polymer to be clean (figure 8).

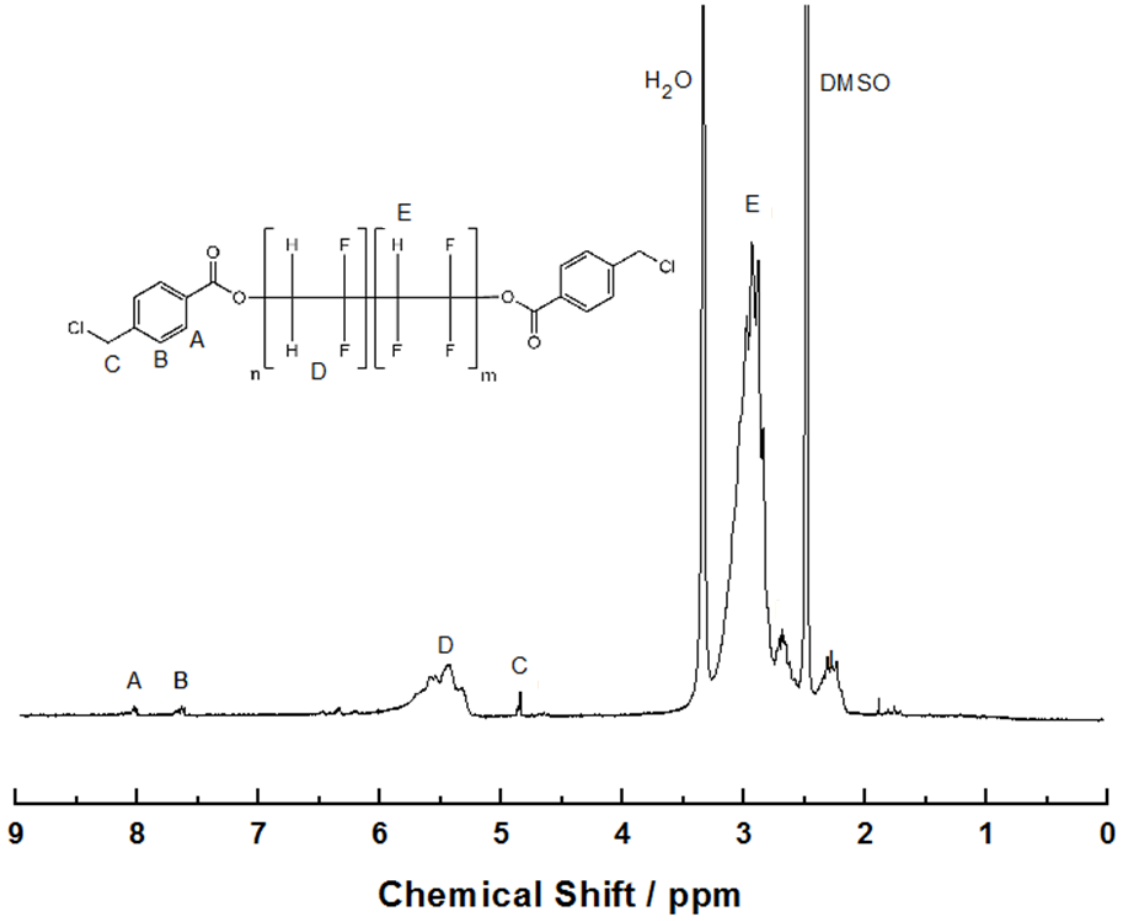

Figure 8: ^{1}H-NMR of P(VDF-TrFE) macro initiator

Besides the assigned peaks in figure 8, peaks at 6.4 and 1.8 correspond to CF_2-H and CF_2-CH_3 groups respectively which result from chain transfer processes (backbiting)[33]. Peaks at 4.6 correspond to hydrogens of the monomer next to the ester group formed with the initiator. Finally, peak D corresponds to the structures of T*r*FE and peaks G, 2.6 and 2.2 correspond to the structures VDF[34].

The ratio of the integrals between peak D (1 hydrogen of T*r*FE) and the combined integrals of peak E, 2.2 and 2.6 of VDF was used to determine the ratio of T*r*FE and VDF and was calculated to be 19% T*r*FE and 81% VDF. GPC measurements of the macro initiator determined that the molecular weight (M_n) was 13 kg/mol and the polydispersity was 1,22. Figure 9 shows the cooling cycle as well as the second heating cycle of the DSC scan of the P(VDF-T*r*FE) macro initiator.

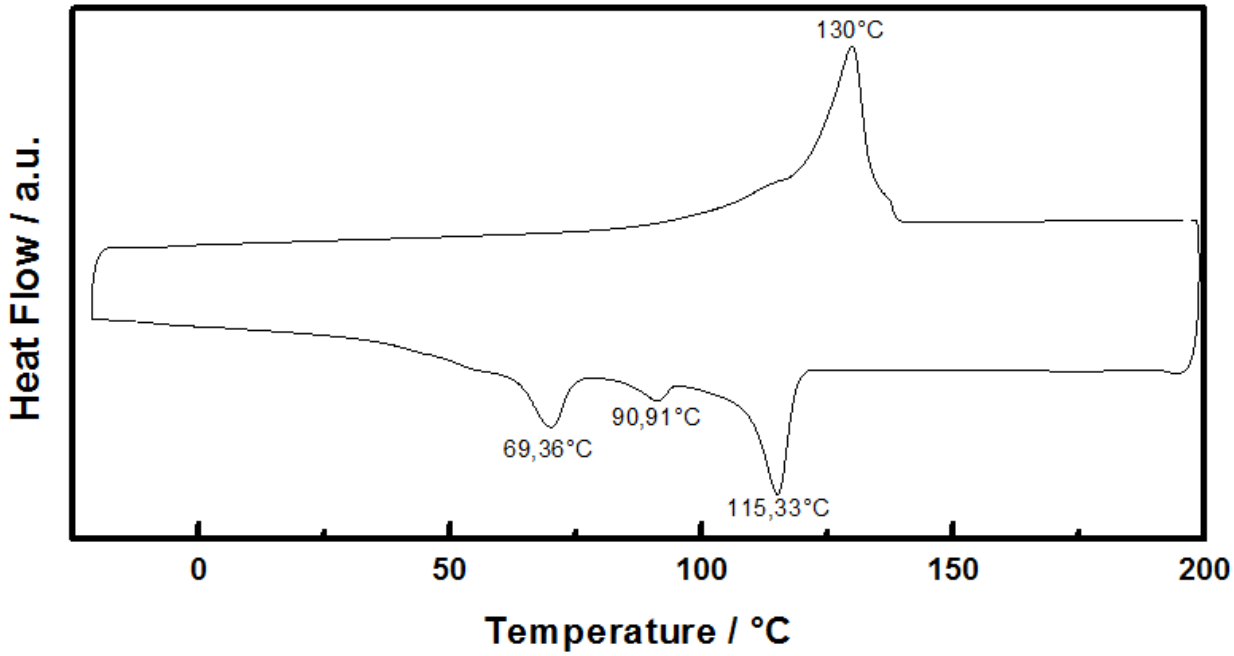

Figure 9: DSC scan of P(VDF-TrFE) macro initiator

The first scan was discarded due to its dependence on the thermal history of the material. Unfortunately, due to the low content of T*r*FE in the polymer, any existing Curie transitions overlap with the melting peak of the material and so the heating scan will not provide any useful information. The cooling scan however shows 3 distinct peaks, a crystallization peak (115°C) and 2 potential curie transitions (90°C and 69°C). This double Curie transition has been observed before[16] and can be explained by the chain formations of the material. It is also possible that one of these peaks is caused by additional crystallization, but this cannot be determined form the DSC alone.

Synthesis of P*t*BMA-*b*-P(VDF-*r*-T*r*FE)-*b*-P*t*BMA block copolymers

A number of block copolymers using the P(VDF-T*r*FE) macro initiator and *t*BMA were synthesized in where the reaction time was systematically varied (Table 1). The conversion was determined using the ^{1}H-NMR spectrum of the quenched reaction mixture (Figure 10) by comparing the integrals of peaks A and B (one hydrogen each of the unreacted monomer) with peak C (three hydrogens of the monomer unit in the polymer) and using equation 1:

$$Conversion = \frac{\frac{1}{2}(\int A + \int B)}{\frac{1}{2}(\int A + \int B) + \frac{1}{3}\int C} * 100$$

Equation 1: conversion calculation

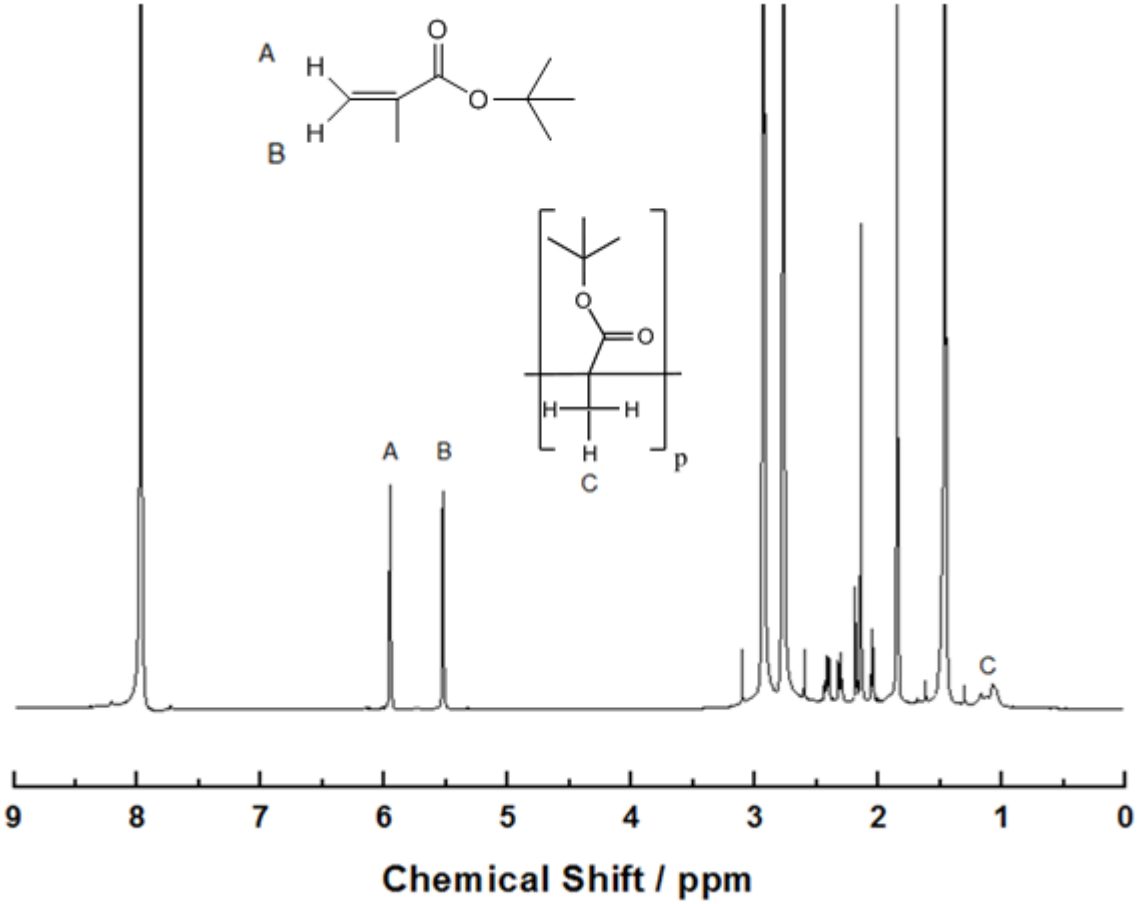

Figure 10: ^{1}H-NMR of the reaction mixture of HHM-006

Entry	Sample	t (h)	Conversion (%)	Yield (g)	f_{Ptbma}	M_n (g/mol)
1*	HHM-003-I	4	12,8	0,4612	0,545	28569,82
2	HHM-004	4	22,7	0,4713	0,668	39120,16
3	HHM-005	6	22,4	0,4925	0,612	33504,12
4	HHM-006	20	28,05	0,763	0,770	56509,07
5	HHM-007	66	49,14	1,118	0,823	73430,71
6	HHM-008	1	17,6	0,348	0,593	31960,17
7	HHM-009	0,5	16,9	0,5469	0,618	34014,15

Table 1: Library of PtBMA-b-P(VDF-r-TrFE)-b-PtBMA copolymers

** HHM-003-I used a newer batch of CuCl*

Unfortunately, the product could not be purified easily by just using precipitation. Especially samples with higher P*t*BMA segments did not precipitate nicely, instead they coagulated together. This was resolved by collecting the coagulated precipitate, dissolving it in acetone and removing the solvent via rotary evaporation. The molecular weight could not be determined directly using GPC, which is a common problem with block copolymers. Instead the weight ratio of the P*t*BMA (f_{Ptbma}) as well as the total molecular weight (M_n) was calculated using the ^{1}H-NMR of the product (Figure 11) and using the following procedure:

1) The integral of A was set to 19 (1H of the T*r*FE part of the macro initiator)
2) The integral of B was calculated and divided by 9 (9H of *t*BMA in polymer)
3) The value calculated at step 2 was used in the following formula at place X, giving the weight ratio of the P*t*BMA blocks in the polymer:

$$f_{\mathrm{Ptbma}} = \frac{X * 142{,}2}{X * 142{,}2 + 81 * 64{,}03 + 19 * 82{,}02}$$

Equation 2: PtBMA ratio calculation

4) Now using the molecular weight of the macro initiator the total molecular weight can be calculated by

$$Mn = 12997{,}5 \,/\, (1 - f_{\mathrm{Ptbma}})$$

Equation 3: Molecular weight calculation of the complete polymer

This method however cannot be used to calculate the polydispersity of the material.

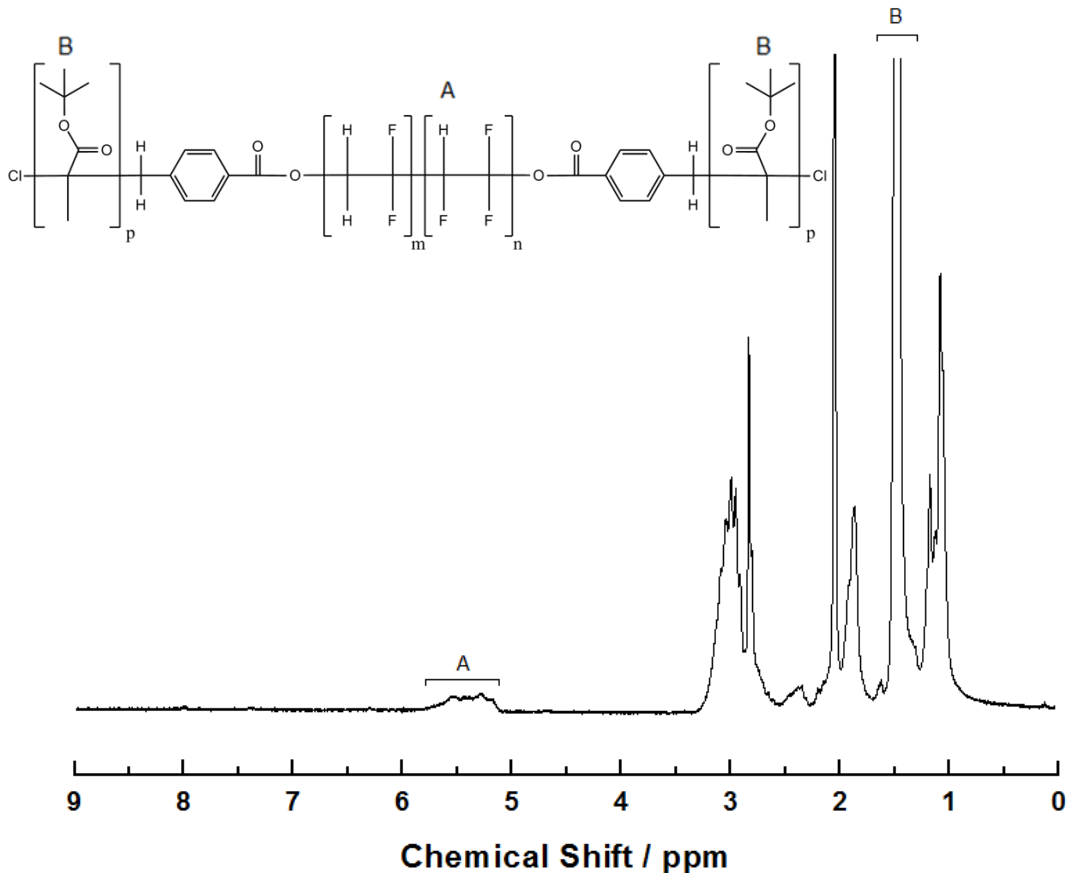

Figure 11: ^{1}H-NMR of HHM-008

The block copolymers were then analyzed using DSC, POM and FTIR. FTIR can be used to determine which phases are present in the P(VDF-T*r*FE) part of the block copolymers[35]. P*t*BMA polymer was synthesized using the previously described procedure for comparison with the block copolymers. Unfortunately, peaks of different P(VDF-T*r*FE) phases overlap with peaks of P*t*BMA making it impossible to determine the phases using FTIR.

DSC measurements were taken of all block copolymers as well as P*t*BMA and were compared. As said before, due to overlapping peaks in the heating cycle only the cooling cycle will be used for comparison. Only the P(VDF-T*r*FE) and P*t*BMA scans were scaled to fit.

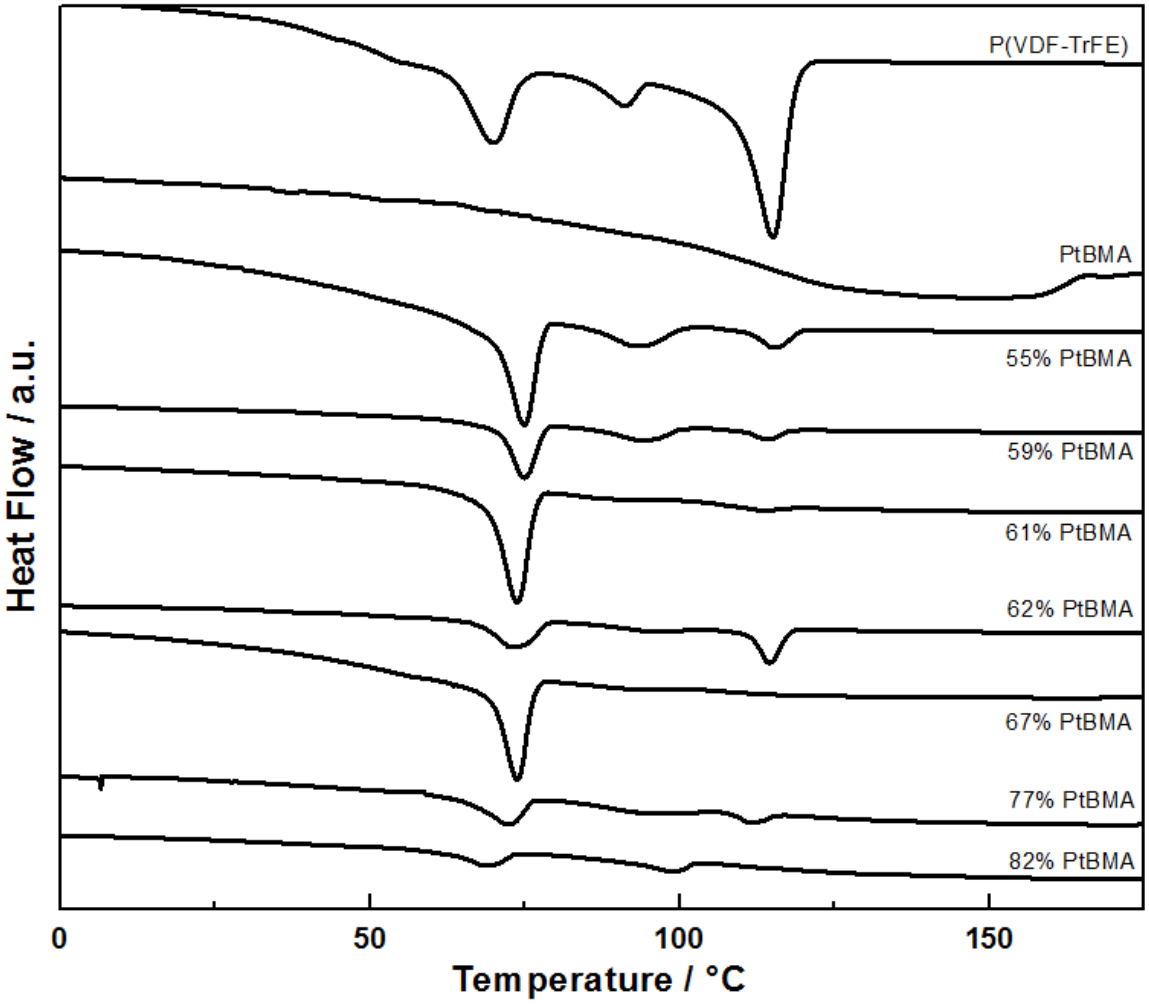

Figure 12: DSC cooling scans of the library of block copolymers, ordered by PtBMA content

The first observation is the significantly reduced crystallization peak in all samples. While this could be caused by the confinement of the crystallization of the P(VDF-T*r*FE), it is also possible that some of the P(VDF-T*r*FE) macroinitiator has not reacted causing this peak. All block copolymers shows peaks at similar temperatures as the P(VDF-T*r*FE) macroinitiator, however the peaks 82% P*t*BMA sample differ, the first peak appears at a slightly lower temperature while the second peak appears at 100°C, which is between the 90°C and 115°C peaks of the P(VDF-T*r*FE) macroinitiator. This shift might be caused by the confinement.

Figure 13 shows solvent cast samples of the P(VDF-T*r*FE) macroinitiator and the 67% P*t*BMA block copolymer. All other block copolymers look similar to the 67% P*t*BMA block copolymer. After comparison of the two images, it is clear that the P(VDF-T*r*FE) macro initiator shows birefringent domains, which are caused by the granular crystals, whereas no crystallization is observer in the sample with 67 wt. % P*t*BMA.

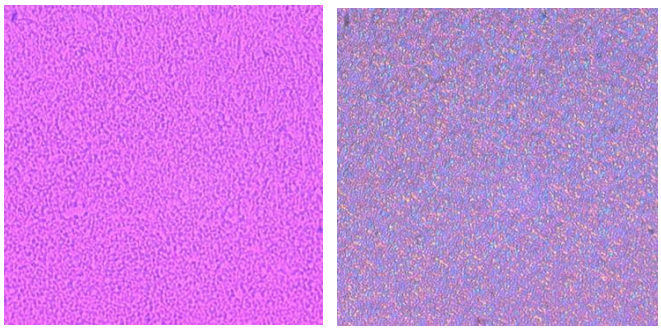

Figure 13: 67% PtBMA block copolymer and macro initiator cast from solvent

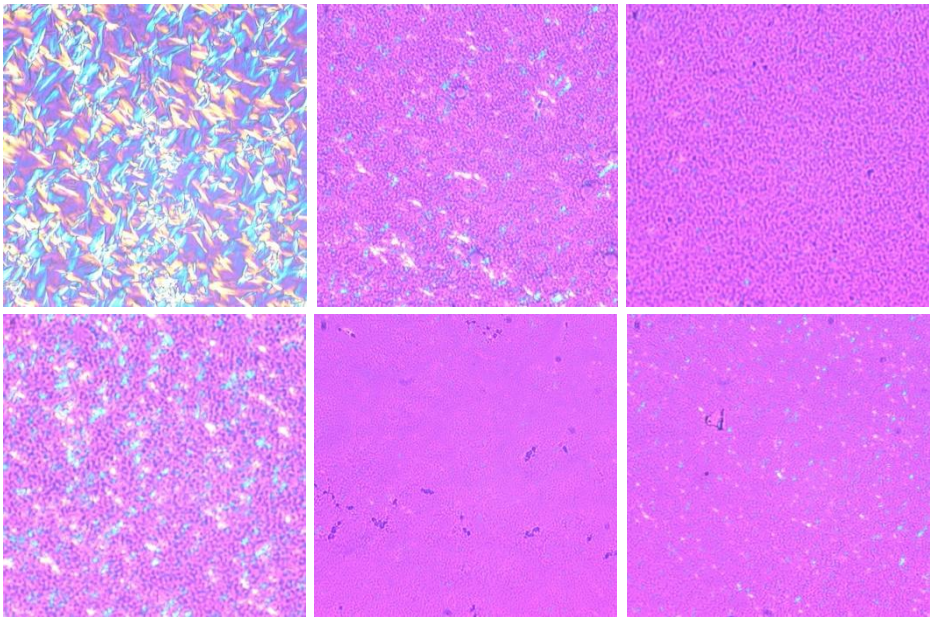

Figure 14: POM images after heating and cooling, from left to right: macroinitiator, 55%, 61%, bottom row: 67%, 77%, 82%

All samples started to crystalize at roughly the temperature of their first peak, even if this peak was barely noticeable on the DSC. No additional crystallization was observed at the temperatures of the other 2 peaks. Additionally, crystallization varied from place to place on the sample so comparison between pictures is unreliable. If the P(VDF-T*r*FE) was confined by the P*t*BMA blocks, no crystallization would show since these domains are too small for the POM to observe. This suggests that the crystallization shown on the POM images is caused by macro separation of unreacted P(VDF-T*r*FE) macroinitiator.

Miscibility of P(VDF-*r*-T*r*FE) and P*t*BMA

The synthesized P*t*BMA was also used to create multiple blends of P*t*BMA with the P(VDF-T*r*FE) macro initiator.

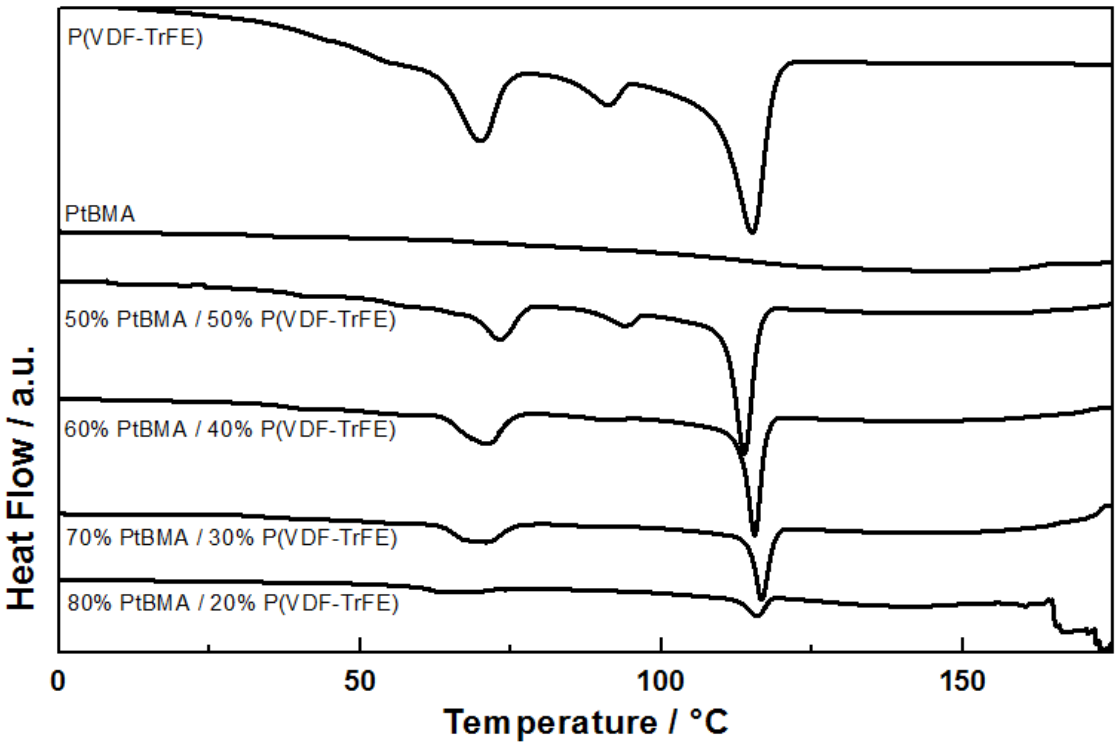

Figure 15: DSC scans of PtBMA/P(VDF-TrFE) blends

The DSC scans from all the blends are similar to the DSC scan of P(VDF-T*r*FE). All the first heating scans show significant noise in the higher temperature range which is the result of evaporation of solvent. Each blend shows a significant crystallization peak at the same temperature as the pure P(VDF-T*r*FE). The DSC samples showed visible macro separation, and the same can be seen on the POM images of all the blends.

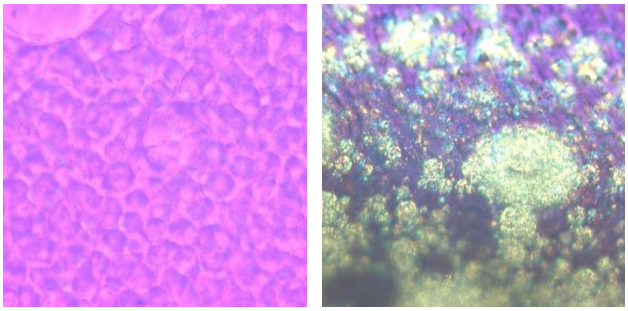

Figure 16: POM images of 80/20 blend

Kinetics of ATRP

ATRP is a controlled radical polymerization; however the results obtained from the synthesis of the block copolymers do not show controlled behavior. HHM-005 reacted 50% longer than HHM-004 yet had a lower conversion and molecular weight than HHM-005. So to determine whether this ATRP reaction is controlled a kinetic study was done. The reaction was done for 48 hours and at pre-determined reaction times 1 ml of reaction mixture was removed to determine conversion via ^{1}H-NMR. In addition, part of this sample was precipitated and the molecular weight and the P(VDF-T*r*FE)/P*t*BMA ratio were determined. Unfortunately for each sample too little product was obtained, therefore purification was challenging. Instead, the ^{1}H-NMR of the impure product was used (Figure 17). This did require some additional mathematics, because one of the peaks of the monomer used to determine conversion overlapped with the multiplet of the T*r*FE protons. To compensate for this, the overall integral of B + C was set to 19 + A. Since A and B are 1 hydrogen each of the unreacted monomer they can be considered equal, allowing us to assume that the integral for C is now 19. This allows us to continue the calculation for the molecular weight as described before.

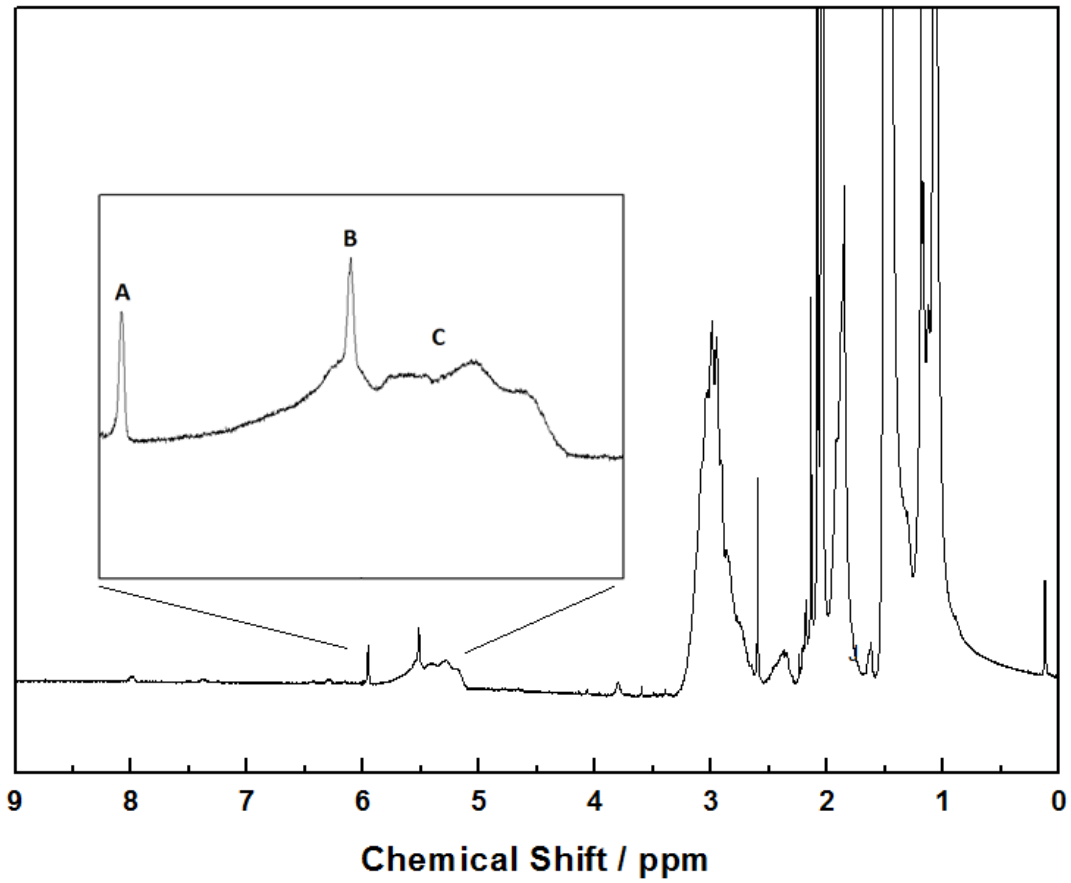

Figure 17: Impure kinetics samples

For each sample, the theoretical molecular weight was calculated using the equation:

$$M_{n,th} = \frac{[M]_0}{[I]} * conversion + M_{P(VDF-TRFE)}$$

Equation 4: Theoretical molecular weight calculation

Both the theoretical as well as measured molecular weights were plotted against the conversion in figure 18. In controlled polymerization the molecular weight scales linearly with the conversion of monomer, and this is what we observe here. However the theoretical values for the molecular weight are roughly 3-3,5 times bigger than the observed values. This indicates that the P(VDF-T*r*FE) macro initiator used has a low initiation speed. Lower initiation rates will cause the polydispersity to increase, and if the initiation rate is too low, some of the initiator will not react.

t (h)	Conv (%)	M_n (g/mol)	f_{Ptbma}
0	3,18	14576,0908	0,1083
0,58	16,62	27235,5452	0,522774
1	16,92	28890,0529	0,550105
2	18,69	28650,553	0,546344
4	19,76	32003,8534	0,593877
24	38,53	48485,3653	0,731929
48	42,4	49643,7014	0,738184

Table 2: Kinetics samples of ATRP

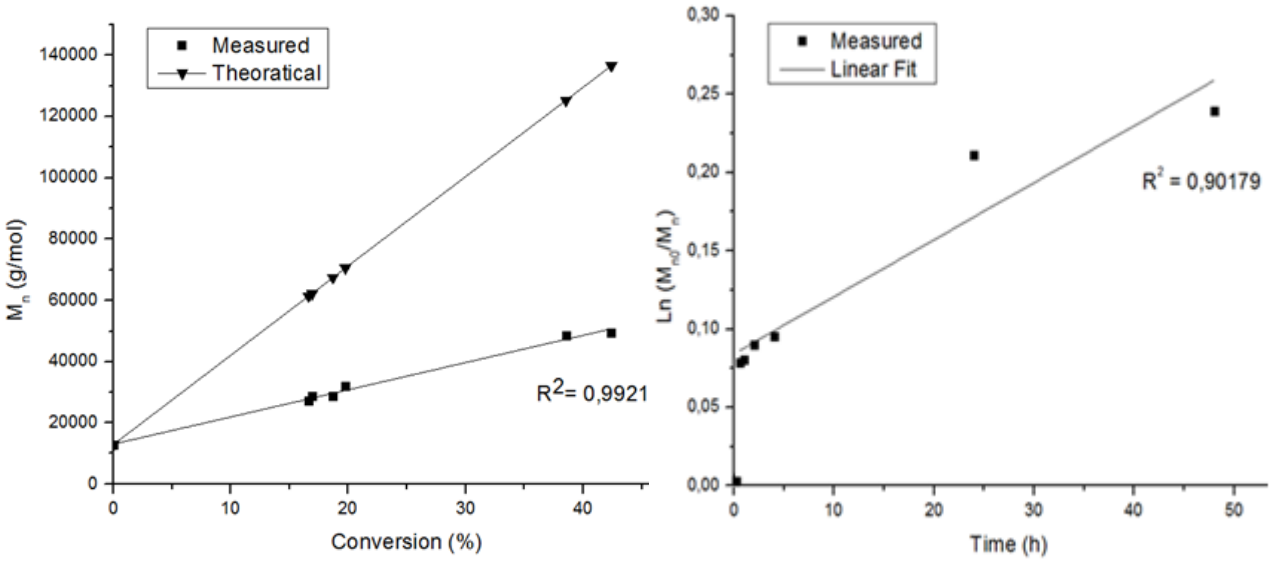

Figure 18: Molecular weight against conversion (left) and ln(M_0/M) against time (right) of PtBMA-b-P(VDF-r-TrFE)-b-PtBMA ATRP

Conclusions

A P(VDF-*r*-T*r*FE) macro initiator was synthesized and used to initiate ATRP reactions with *t*BMA using a Cu(I)Cl catalyst with PMDETA ligands, resulting in a library of P*t*BMA-*b*-P(VDF-*r*-T*r*FE)-*b*-P*t*BMA block copolymers. DSC scans of these block copolymers show peaks at similar temperatures as the pure macro initiator. However the crystallization peaks were of a much smaller intensity. POM measurements show reduced but visible crystallization. These results combined with unreliable predictability of the molecular weight during synthesis led to kinetic study, which suggested that the rate of initiation of the P(VDF-*r*-T*r*FE) macroinitiator was low, which suggests that all of the synthesized block copolymers still contain P(VDF-*r*-T*r*FE) macroinitiator. In order to properly study P*t*BMA-*b*-P(VDF-*r*-T*r*FE)-*b*-P*t*BMA block copolymers, a different synthesize method is required. Click chemistry uses an azide-alkyne reaction to couple 2 polymer blocks[29]. This reaction would allow for better control of the P*t*BMA block and since it a different kind of reaction it would not suffer from the low initiation problem that ATRP has shown. Analyzing the block copolymers with small-angle X-ray scattering (SAXS) and transmission electron microscopy (TEM) would give more information on the self-assembly itself.

Acknowledgement

First, I would like to thank Niels Meereboer for being a great supervisor, as well as Katja Loos for allowing me to do my bachelor thesis in her group. I also thank Ivan Terzic for his help during this research and Anton Hofman for the GPC measurements. Finally, I would like to thank Jin Xu, Quiyan Yang and Csaba Fodor for their suggestions for the final presentation.

References

1. Kao, K.-C. *Dielectric phenomena in solids with emphasis on physical concepts of electronic processes*. 2004; Available from: http://site.ebrary.com/id/10167034.
2. Lines, M.E. and A.M.j.a. Glass, *Principles and applications of ferroelectrics and related materials*. 1977: Oxford [Eng.] Clarendon Press.
3. Hill, N.A., *Why are there so few magnetic ferroelectrics?* Journal of Physical Chemistry B, 2000. **104**(29): p. 6694-6709.
4. Horiuchi, S. and Y. Tokura, *Organic ferroelectrics.* Nature Materials, 2008. **7**(5): p. 357-366.
5. Kang, S.J., et al., *Nonvolatile polymer memory with nanoconfinement of ferroelectric crystals.* Nano Lett, 2011. **11**(1): p. 138-44.
6. Eerenstein, W., N.D. Mathur, and J.F. Scott, *Multiferroic and magnetoelectric materials.* Nature, 2006. **442**(7104): p. 759-65.
7. Takahashi, Y., et al., *Ferroelectric Switching Characteristics and Crystal Structure of Nylon 11.* Polym J, 1997. **29**(3): p. 234-239.
8. Miyata, S., et al., *PIEZOELECTRICITY REVEALED IN THE CO-POLYMER OF VINYLIDENE CYANIDE AND VINYL-ACETATE.* Polymer Journal, 1980. **12**(12): p. 857-860.
9. Poulsen, M. and S. Ducharme, *Why Ferroelectric Polyvinylidene Fluoride is Special.* Ieee Transactions on Dielectrics and Electrical Insulation, 2010. **17**(4): p. 1028-1035.
10. Lovinger, A.J., *FERROELECTRIC POLYMERS.* Science, 1983. **220**(4602): p. 1115-1121.
11. Sencadas, V., R. Gregorio Filho, and S. Lanceros-Mendez, *Processing and characterization of a novel nonporous poly(vinilidene fluoride) films in the β phase.* Journal of Non-Crystalline Solids, 2006. **352**(21-22): p. 2226-2229.
12. Gregorio, R. and D.S. Borges, *Effect of crystallization rate on the formation of the polymorphs of solution cast poly(vinylidene fluoride).* Polymer, 2008. **49**(18): p. 4009-4016.
13. Ameduri, B., *From Vinylidene Fluoride (VDF) to the Applications of VDF-Containing Polymers and Copolymers: Recent Developments and Future Trends.* Chemical Reviews, 2009. **109**(12): p. 6632-6686.
14. Koga, K. and H. Ohigashi, *Piezoelectricity and related properties of vinylidene fluoride and trifluoroethylene copolymers.* Journal of Applied Physics, 1986. **59**(6): p. 2142-2150.
15. Furukawa, T., *Structure and functional properties of ferroelectric polymers.* Advances in Colloid and Interface Science, 1997. **71-2**: p. 183-208.
16. Gregorio, R. and M.M. Botta, *Effect of crystallization temperature on the phase transitions of P(VDF/TrFE) copolymers.* Journal of Polymer Science Part B: Polymer Physics, 1998. **36**(3): p. 403-414.
17. Lutkenhaus, J.L., et al., *Confinement Effects on Crystallization and Curie Transitions of Poly(vinylidene fluoride-co-trifluoroethylene).* Macromolecules, 2010. **43**(8): p. 3844-3850.
18. Cauda, V., et al., *Nanoconfinement: an effective way to enhance PVDF piezoelectric properties.* ACS Appl Mater Interfaces, 2013. **5**(13): p. 6430-7.
19. Serghei, A., et al., *Curie transitions for attograms of ferroelectric polymers.* Nano Lett, 2013. **13**(2): p. 577-80.
20. Kassa, H.G., et al., *The Ferro- to Paraelectric Curie Transition of a Strongly Confined Ferroelectric Polymer.* Macromolecules, 2014. **47**(14): p. 4711-4717.
21. Bates, F.S. and G.H. Fredrickson, *Block Copolymers—Designer Soft Materials.* Physics Today, 1999. **52**(2): p. 32.
22. Botiz, I. and S.B. Darling, *Optoelectronics using block copolymers.* Materials Today, 2010. **13**(5): p. 42-51.
23. Loo, Y.L., R.A. Register, and A.J. Ryan, *Modes of crystallization in block copolymer microdomains: Breakout, templated, and confined.* Macromolecules, 2002. **35**(6): p. 2365-2374.
24. Thomas, E.L., et al., Macromolecules, 1986. **19**: p. 5.

25. Zheng, W. and Z.-G. Wang, *Morphology of ABC Triblock Copolymers.* Macromolecules, 1995. **28**(21): p. 7215-7223.
26. Olsen, B.D. and R.A. Segalman, *Self-assembly of rod–coil block copolymers.* Materials Science and Engineering: R: Reports, 2008. **62**(2): p. 37-66.
27. He, W.-N. and J.-T. Xu, *Crystallization assisted self-assembly of semicrystalline block copolymers.* Progress in Polymer Science, 2012. **37**(10): p. 1350-1400.
28. Chanthad, C., et al., *Synthesis of triblock copolymers composed of poly(vinylidene fluoride-co-hexafluoropropylene) and ionic liquid segments.* J. Mater. Chem., 2012. **22**(2): p. 341-344.
29. Voet, V.S.D., G. ten Brinke, and K. Loos, *Well-defined copolymers based on poly(vinylidene fluoride): From preparation and phase separation to application.* Journal of Polymer Science Part A: Polymer Chemistry, 2014. **52**(20): p. 2861-2877.
30. Matyjaszewski, K. and J.H. Xia, *Atom transfer radical polymerization.* Chemical Reviews, 2001. **101**(9): p. 2921-2990.
31. Krzysztof, M., *Overview: Fundamentals of Controlled/Living Radical Polymerization*, in *Controlled Radical Polymerization*. 1998, American Chemical Society. p. 2-30.
32. Voet, V.S.D., et al., *Block copolymer route towards poly(vinylidene fluoride)/poly(methacrylic acid)/nickel nanocomposites.* RSC Advances, 2013. **3**(21): p. 7938.
33. Pianca, M., et al., *End groups in fluoropolymers.* Journal of Fluorine Chemistry, 1999. **95**(1-2): p. 71-84.
34. Yagi, T. and M. Tatemoto, *A Fluorine-19 NMR Study of the Microstructure of Vinylidene Fluoride-Trifluoroethylene Copolymers.* Polym J, 1979. **11**(6): p. 429-436.
35. Jin, X.Y., K.J. Kim, and H.S. Lee, *Grazing incidence reflection absorption Fourier transform infrared (GIRA-FTIR) spectroscopic studies on the ferroelectric behavior of poly(vinylidene fluoride–trifluoroethylene) ultrathin films.* Polymer, 2005. **46**(26): p. 12410-12415.